Local-Scale Simulations of Nucleate Boiling on Micrometer Featured Surfaces

Preprint

Hariswaran Sitaraman, Gilberto Moreno, and Sreekant Narumanchi
National Renewable Energy Laboratory

Ercan M. Dede, Shailesh N. Joshi, and Feng Zhou
Toyota Research Institute of North America

Presented at the ASME Summer Heat Transfer Conference
Bellevue, Washington
July 9–14, 2017

NREL is a national laboratory of the U.S. Department of Energy
Office of Energy Efficiency & Renewable Energy
Operated by the Alliance for Sustainable Energy, LLC

This report is available at no cost from the National Renewable Energy Laboratory (NREL) at www.nrel.gov/publications.

Conference Paper
NREL/CP-2C00-68294
August 2017

Contract No. DE-AC36-08GO28308

NOTICE

This report is available at no cost from the National Renewable Energy Laboratory (NREL) at www.nrel.gov/publications.

Available electronically at SciTech Connect http:/www.osti.gov/scitech

Available for a processing fee to U.S. Department of Energy and its contractors, in paper, from:

U.S. Department of Energy
Office of Scientific and Technical Information
P.O. Box 62
Oak Ridge, TN 37831-0062
OSTI http://www.osti.gov
Phone: 865.576.8401
Fax: 865.576.5728
Email: reports@osti.gov

Available for sale to the public, in paper, from:

U.S. Department of Commerce
National Technical Information Service
5301 Shawnee Road
Alexandria, VA 22312
NTIS http://www.ntis.gov
Phone: 800.553.6847 or 703.605.6000
Fax: 703.605.6900
Email: orders@ntis.gov

Cover Photos by Dennis Schroeder: (left to right) NREL 26173, NREL 18302, NREL 19758, NREL 29642, NREL 19795.

NREL prints on paper that contains recycled content.

Proceedings of ASME Summer Heat Transfer Conference
SHTC2017
July 9-14, 2017, Bellevue, Washington, USA

HT2017-4710

LOCAL-SCALE SIMULATIONS OF NUCLEATE BOILING ON MICROMETER-FEATURED SURFACES

Hariswaran Sitaraman
National Renewable Energy Laboratory
Golden, CO, USA

Gilberto Moreno
National Renewable Energy Laboratory
Golden, CO, USA

Ercan M. Dede
Toyota Research Institute of North America
Ann Arbor, MI, USA

Shailesh N. Joshi
Toyota Research Institute of North America
Ann Arbor, MI, USA

Feng Zhou
Toyota Research Institute of North America
Ann Arbor, MI, USA

Sreekant Narumanchi
National Renewable Energy Laboratory
Golden, CO, USA

ABSTRACT

A high-fidelity computational fluid dynamics (CFD)-based model for bubble nucleation of the refrigerant HFE7100 on micrometer-featured surfaces is presented in this work. The single-fluid, incompressible Navier-Stokes equations, along with energy transport and natural convection effects, are solved on a featured surface resolved grid. An *a priori* cavity detection method is employed to convert raw profilometer data of a surface into well-defined cavities. The cavity information and surface morphology are represented in the CFD model by geometric mesh deformations. Surface morphology is observed to initiate buoyancy-driven convection in the liquid phase, which in turn results in faster nucleation of cavities. Simulations pertaining to a generic rough surface show a trend where smaller size cavities nucleate with higher wall superheat. This local-scale model will serve as a self-consistent connection to larger device scale continuum models where local feature representation is not possible.

1. INTRODUCTION

Multiphase heat transfer through boiling is commonly employed as a cooling technology in several applications, including refrigeration and cooling of electronics and power generation systems. This cooling technique is superior when compared to single-phase techniques, mainly due to the energy associated with liquid to vapor phase change. The heat transfer rates are more pronounced in the nucleate boiling regime because of bubble nucleation, motion, and condensation. Consequently, nucleate boiling-based heat transfer is increasingly being considered for electronics thermal management to obtain high performance and reliability from components with reduced footprint and weight. Advances in modeling tools for two-phase heat transfer are required to help with time- and cost-effective design of high-performance thermal management systems.

Bubble nucleation is the process by which gas bubbles are formed in a liquid at supercritical/superheated temperatures. Nucleation via phase change during boiling is one of several examples. Gas bubble formation in aerated liquids under supercritical conditions is another example and has equal practical importance in several industrial processes such as foaming of liquid plastics and steam generation [1]. Nucleation is generally classified as being either homogeneous or heterogeneous. In homogenous nucleation, the liquid is

perfectly wetting on bounded surfaces, and nucleation happens within the bulk of the liquid phase. Heterogeneous nucleation is observed when the liquid phase has a finite contact angle with the surface; this creates vapor/gas pockets in surface cavities that serve as seeds for bubble formation. Bubble nucleation in supercritical liquids can sometimes result in explosive boiling, which is a major safety concern in nuclear reactors, paper processing and cryogenic systems [2]. It is well known that boiling surface characteristics (i.e., nanometer and micrometer surface features) significantly influence boiling heat transfer coefficients, critical heat flux, and boiling incipience superheat. Several researchers have explored the enhancement of boiling heat transfer via surface features. Jacob and Fritz performed one of the earliest studies on the effect of surface roughness on nucleate boiling in 1931 [3]. Since then, several studies in the late 1960s and 1970s aimed at developing artificially enhanced surfaces to improve boiling heat transfer [4-5]. For example, Webb in 1972 [6] engineered an enhanced surface with bent fins that gave high boiling heat transfer coefficients. A generally accepted model for average heat flux during nucleate boiling from conventional theory predicts a direct dependence on nucleation site density, bubble departure diameter, and bubble departure frequency [7]. Among these, the nucleation site density is a function of wall superheat, saturation temperature, latent heat, and vapor density. The surface features in turn affect the onset of nucleate boiling which has been extensively studied through boiling curves obtained from experiments [8-12].

The boiling curve, which is a plot of heat flux versus wall superheat, has four widely accepted regions [13]. The first region at low wall superheat is where heat transfer is dominated by natural convection and conduction in the liquid phase. The slope of the curve starts to increase in the second region at slightly higher wall superheat when discrete bubbles start forming at surface cavities. Fully developed nucleate boiling is observed in the third region at higher superheats, where nucleation site density is the maximum and the heat transfer coefficient is the highest. The fourth and the final region is where coalesced bubbles near the surface result in a vapor film, which results in the maximum attainable heat flux; this is referred to as critical heat flux (CHF). The first two aforementioned regions play an important role in determining the boiling regime and are the focus of this work.

Recent experimental work by several groups has emphasized delaying CHF by engineering surface features; Das et al. [9,14] used structured and tunneled surfaces along with imposed fluid rotations and appreciable enhancements in heat transfer in the nucleate boiling regime were observed. Micro/nano porous and coated surfaces have also been also studied. Jung et al. [15] observed 2 to 3 times enhancement on copper-coated surfaces with varying surface orientations. Surfaces with nanowires/nanotube-like features have also shown a similar factor in heat transfer improvements [16].

Current modeling tools for boiling heat transfer simulate physics on a facet of the large range of length and time scales associated with the phenomenon. Figure 1 shows a summary of existing modeling strategies and highlights the methodology used in this work. Most of the currently available modeling tools operate at the scale of several millimeters (several bubble diameters) to large device length scales. The former is usually simulated using volume of fluid (VOF) approach where bubble interphases are tracked and resolved. Simulations of boiling heat transfer at large length scales are performed using multiphase Euler approach where intermixing of phases are modeled without sharp interphase tracking. These tools however lack the ability to accurately model the sensitive effects of heated surface conditions/roughness on boiling heat transfer, which occurs at very small length scales; thus, correlation-based approaches "tuned" from experimental measurements are used instead. This work addresses this particular issue, thereby paving the way to a self-consistent, parameter-free model for larger-length-scale simulations.

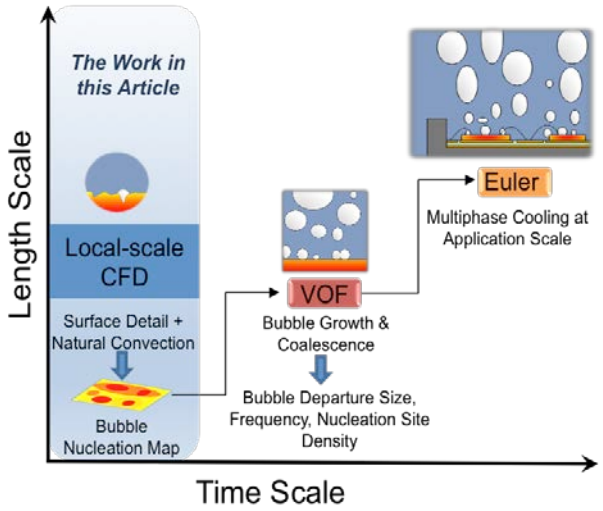

FIGURE 1: DIFFERENT MODELING METHODOLOGIES FOR SIMULATING BOILING PHENOMENON AT VARIOUS LENGTH AND TIME SCALES.

Several VOF-based CFD models have been used to study bubble departure diameter and frequency. Kunkelmann and Stephan [17] used a VOF solver to study bubble departure diameters and frequency for nucleate boiling of the dielectric fluid HFE7100. A thin film microlayer model was used in the near wall interphase, which couples with the macrolayer model via heat and mass fluxes. Fang et al. [18] used a VOF-based model to study vapor venting in micro-channels. Wu et al. [19] studied sub-cooled nucleate boiling using a level-set method with a microlayer model based on lubrication theory for the interfacial near-wall region. Ling et al. [20] used a VOF level set approach to simulate bubble motion and coalescence in nucleate boiling with a uniform distribution of active nucleation sites. All of the above-mentioned studies use an imposed initial

gas fraction based on a chosen bubble distribution. These simulations determine important parameters such as bubble departure diameter and frequency that determine average heat flux during nucleate boiling, but the nucleation site density, which depends strongly on the surface morphology, is not resolved. Probabilistic representation of rough surfaces and initiation of bubbles based on thermodynamic considerations have been recently explored by several researchers. Yazdani et al. [21] performed simulations of pool boiling using a VOF model with a stochastic representation of nucleation on rough surfaces. A probability distribution function was used to obtain cavity size at a given location with subsequent application of the critical superheat criterion for bubble nucleation. Sato and Niceno [22] employed a random generation of nucleation sites on a generic rough surface with experimentally derived activation temperatures for nucleation. Liu and Hughes [23] solved single-fluid, compressible Navier-Stokes-Korteweg equations to perform simulations of nucleate and film boiling with random temperature perturbations on the heated surface to represent nucleation sites.

Multiphase Euler models have also been used to study boiling heat transfer at device length scales. Narumanchi et al. [24] studied nucleate boiling of impinging jets using a multiphase Euler model. Here, surface features and bubble interphases were not resolved, and a model for interphase heat and mass transfer using the Ranz-Marshall correlation [25] was used. Li et al. [26] performed a validation study of nucleate boiling in heated pipes using an Eulerian multiphase model. Reasonable agreement with experiments was obtained using correlation-based models for nucleation site density, bubble departure diameter, and frequency.

There have been several studies pertaining to nucleate boiling at small length scales using particle-based approaches as opposed to continuum models. Gong and Cheng [27] employed a lattice Boltzmann methodology to simulate nucleate boiling of a single bubble from a microscale-heated surface. This method does not require an imposed initial bubble profile, and interphase capturing is self-consistently handled by solving the density distribution functions. This approach, although self-contained, is computationally very expensive for large problem sizes and high Reynolds numbers. Maruyama and Kimura [28] studied bubble nucleation using molecular dynamics simulations, including studying boiling of liquid argon between two solid surfaces represented by layers of molecules. The system was expanded at constant temperature; formation of a spherical lower density region was observed, which represents the formation of a vapor bubble. These simulations capture nucleation physics at the molecular level. However, these calculations operate on picosecond time scales and length scales on the order of several angstroms. In 1962, Hsu [29] developed an asymptotic model to predict limiting cavity sizes using one-dimensional transient heat conduction and the Clausius-Clapeyron equation. This model predicts the waiting time for a vapor pocket in a cavity to grow out and become a bubble. This framework gave good predictions with regard to likelihood of nucleation for a given cavity size. We extend this approach in this work using fully resolved CFD simulations.

The contributions of this work are as follows.

1) A multi-dimensional extension to the theoretical framework developed by Hsu [29] is expanded to study nucleation on a generic surface.
2) The CFD-based model built on Hsu's approach is of higher fidelity in several aspects as listed below.
    a. The proposed model is able to capture three-dimensional (3-D) effects.
    b. The surface features are resolved.
    c. Natural convection and conduction effects are accounted for in the model.
    d. The thermal boundary layer is self-consistently captured as opposed to the use of a constant value derived from correlations.
    e. Cavity nucleation for a generic featured surface is captured in a temporally accurate manner as opposed to obtaining limiting cavity sizes.
3) A cavity detection method is developed to convert raw profilometer data of a generic surface into well-defined cavities.

2. MATHEMATICAL MODEL

The incompressible Navier-Stokes equations along with the energy equation using the single-fluid formulation are used to solve for the fluid dynamics of nucleate boiling phenomenon. The phase-averaged momentum, continuity, and energy equations are shown in Equations (1), (2) and (3), respectively.

$$\frac{\partial \boldsymbol{u}}{\partial t} + (\boldsymbol{u}.\boldsymbol{\nabla})\boldsymbol{u} = -\frac{\boldsymbol{\nabla} p}{\rho} + \boldsymbol{\nabla}.(\nu(\boldsymbol{\nabla}\boldsymbol{u} + \boldsymbol{\nabla}\boldsymbol{u}^T)) - \beta(T - T_0)\boldsymbol{g} \quad (1)$$

$$\boldsymbol{\nabla}.\boldsymbol{u} = 0 \quad (2)$$

$$\rho C\left(\frac{\partial T}{\partial t} + \boldsymbol{u}.\boldsymbol{\nabla}T\right) = \boldsymbol{\nabla}.(k\boldsymbol{\nabla}T) \quad (3)$$

Here $\boldsymbol{u}$ represents the fluid velocity vector, p is the pressure, ρ is the average density, ν and β represent the kinematic viscosity and the volume thermal expansion coefficient, respectively, C is the average specific heat, T is the temperature, and k is the mixture-averaged thermal conductivity. This model differs from VOF and other multiphase models in the sense that interfaces are not captured and not present at the beginning of the simulation. The gas fraction in the domain changes by instantaneous activation of surface cavities based on the bubble

nucleation criterion discussed in Section 2.1. This is a reasonable approach in the early stages of boiling, where natural convection and conduction heat transfer in the liquid phase alone aid in the initiation of vapor bubbles in the surface cavities. A well-established CFD code, Nek5000 [30], is used in this work. This solver uses a higher-order spectral finite element discretization on general unstructured hexahedral meshes; higher-order methods can resolve small fluid length scales with minimal dispersion errors giving it a direct numerical simulation capability.

Local-scale micrometer-size features on the solid surface are handled using the mesh deformation facility in the solver at run time. The featured surface data are read as an input file, and appropriate deformation is applied by interpolating surface data to grid points. The Boussinesq approximation is used in this work. This results in the natural convection source term in the momentum equation that depends on the volumetric thermal expansion coefficient of the liquid. The transport properties are obtained using volume-fraction-weighted averaging given by Equation 4:

$$\mu = \alpha_l \mu_l + (1 - \alpha_l)\mu_g \tag{4}$$

Here μ, μ_l, and μ_g represent transport properties that include viscosity, thermal conductivity and specific heat for the fluid mixture, liquid, and gas, respectively.

2.1 Nucleation Model

The nucleation model used in this study is similar to the approach presented by Hsu [29], where a thermodynamic criterion is applied in conjunction with geometry information of the cavity. Figure 2 shows the schematic of a spherical bubble nucleated on a cavity. The cavity is assumed to have a rounded edge at its mouth. This essentially decouples the dependence of angle, ϕ, on the depth and cone angle of the cavity. The angle ϕ here reduces to the interface contact angle, which is a fluid property independent of geometry. The height, h, of the bubble depends on geometric parameters, including the fluid contact angle (ϕ) and the cavity radius (R_c). The radius of the bubble, R, and the cavity radius, R_c, are related by $R_c = Rsin\phi$. A cavity is nucleated when the temperature at the tip of the spherical bubble at height h (in Figure 2) exceeds the critical value predicted by the combination of Clausius-Clapeyron and Young-Laplace equation given by Equation 5:

$$T_b = T_s + \frac{2\sigma T_s}{RL\rho_g} \tag{5}$$

Here, T_b is the critical bubble temperature, T_s is the saturation temperature, σ is the surface tension, L is the latent heat, and ρ_g is the vapor density. The bubble height, h can be related to the cavity radius through geometrical constraints and is given by Equation 6:

$$h = \frac{R_c(1+cos\phi)}{sin\phi} \tag{6}$$

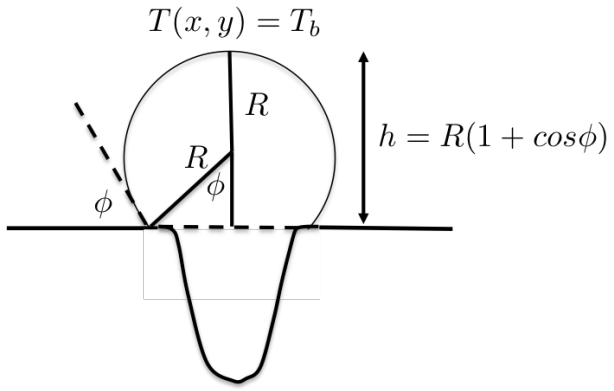

FIGURE 2: SCHEMATIC OF BUBBLE NUCLEATION IN A CAVITY. HERE ϕ REPRESENTS THE CONTACT ANGLE, R REPRESENTS THE BUBBLE RADIUS, $T(x,y)$ REPRESENTS THE TEMPERATURE FIELD, AND h REPRESENTS THE BUBBLE HEIGHT FROM THE SURFACE.

Nucleation is imposed by instantaneous increase of the vapor volume fraction (α_g) at the nucleating cavity in a spherically shaped region of radius, R. This in turn changes the viscosity and thermal conductivity in this region, thereby affecting momentum and energy transport. It should be noted that heterogeneous nucleation is a molecular phenomenon that depends on surface wettability and fluid contact angle at smaller than micrometer length scales. A simplistic assumption similar to the work done by Hsu [29] is made, where a vapor pocket is assumed to be present in every cavity. The assumption of critical temperature attainment at the tip of the bubble ensures that there is enough superheat to sustain the growth of the vapor pocket into a stable bubble on top of the cavity. An absolutely realistic simulation should use a VOF approach at the sub-micrometer cavity length scale to simulate the growth of the vapor pocket; however, this approach will require extremely high resolution, and it becomes intractable to simulate domains of large length scales on the order of several millimeters.

2.2 Cavity Detection Method

Cavity information was obtained for a copper sandpaper-polished surface (600 grit sandpaper) using a laser profilometer (Keyence laser profilometer and surface metrology software *TrueMap*). The profilometer scanned a 2×2 mm^2 area of the copper surface to obtain topography information. The profilometer information was then imported into *TrueMap* software to estimate the cavity sizes and locations. Multiple planes parallel to the surface were analyzed to detect voids (i.e., cavities and scratches). The size and centroid location of the cavities were measured. Because cavities have a depth associated with them, this process could potentially detect the same cavity at different horizontal planes. Therefore, duplicate

cavities were eliminated by evaluating the cavity centroid location. If the cavity centroids at different planes were found to be within 150 μm of one another, the cavities were considered the same and its centroid location at the highest plane was used (i.e., the cavity at the highest plane was assumed to be the cavity opening). This analysis provided cavity surface area information, which was converted to an equivalent diameter assuming a circular opening (i.e., mouth). This image processing approach represents an attempt to estimate cavities on the surface using some simplifying assumptions. In reality, the surface cavities and scratches are irregular in shape, and the cavity opening is likely slanted (i.e., not entirely on the one horizontal plane). Nonetheless, it may be possible to extend the framework of the technique, with some modifications, to complex 3-D surface topographies (e.g., porous coated surface structures) considering the current state of the art in image processing.

Figure 3(a) shows the raw profilometer data, and Figure 3(b) shows the distribution of cavities found from the application of the detection method mentioned above. The smallest and largest cavity sizes are on the order of 2 μm and 300 μm, respectively. The distribution (Figure 3(c)) shows a large number of cavities in the small diameter range of approximately 0–8 μm. Most of the cavities are present within the 50-μm range for this surface. Only about four cavities exceed 100 μm in size.

2.3 Transport Properties

The thermodynamics and transport properties used in this work are shown in Table 1. The properties are assumed to be constant with respect to temperature; this assumption is reasonable for relatively small superheats ~5–10 K used in this study. For example, the liquid density, specific heat, and viscosity variations are within 10% for a 10 K rise in temperature.

TABLE 1: THERMODYNAMIC AND TRANSPORT PROPERTIES OF HFE7100 USED IN THE MODEL.

Property	Liquid	Vapor
Saturation temperature (K)	333.15[1]	
Density (kg/m^3)	1,371.94[1]	9.66[1]
Specific heat (J/K/kg)	1,253.8[1]	199.5[2]
Viscosity (kg/m/s)	3.5e-4[1]	1.4e-5[3]
Thermal conductivity (W/m/K)	0.062[1]	0.01[3]
Surface tension (N/m)	0.0117[1]	
Latent heat of vaporization (kJ/kg)	112.1[1]	
Thermal expansion coefficient (K^{-1})	0.003[1]	
Bubble contact angle (degrees)	30[4]	

[1] Mudawar thermal systems – NREL Subcontract Report [31]
[2] Computed using specific heat ratio = 1.2 [32] and molecular weight = 250
[3] Verbal communications with 3M
[4] Kunkelmann, 2011 [33]

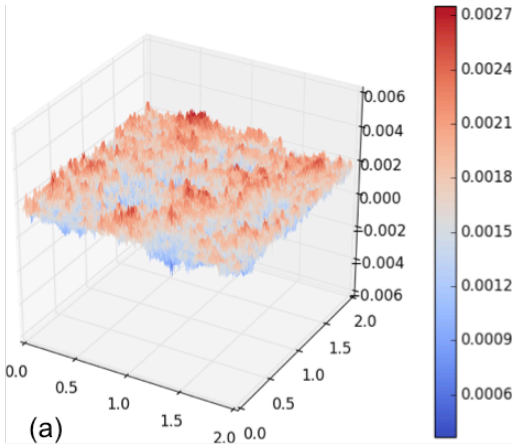

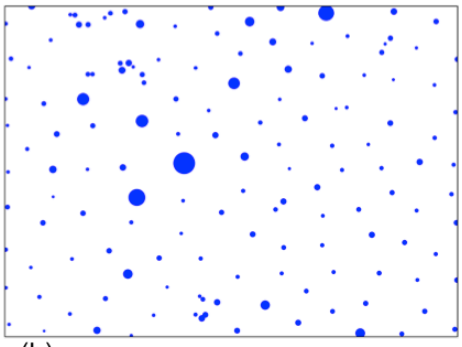

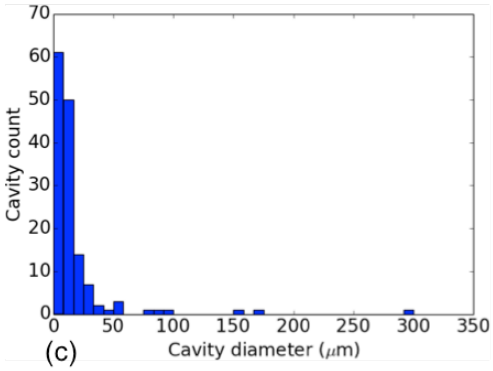

FIGURE 3: (a) RAW PROFILOMETER DATA FOR THE SAND PAPER POLISHED SURFACE, ALL DIMENSIONS ARE IN MILLIMETERS, AND THE SURFACE IS COLORED BY FEATURE HEIGHT (mm) IN THE OUT-OF-PLANE DIRECTION; (b) SHOWS THE CAVITY MAP ON THE 2X2 mm^2 SURFACE ALONG WITH RELATIVE CAVITY SIZES; (c) SHOWS THE CAVITY SIZE DISTRIBUTION HISTOGRAM.

3. RESULTS AND DISCUSSION

The simulation results pertaining to a specific configuration of cavities is first presented to highlight the importance of natural convection and conduction in the bubble nucleation process. The second half of this section pertains to

bubble nucleation on a generic rough surface, where the cavity detection method described in Section 2.2 is utilized.

3.1 Nucleation on a Featured Surface

Figure 4 shows the geometry and computational mesh used in the baseline simulations with a chosen cavity distribution. A regular box mesh, as shown in Figure 4(a), is first created, and the cavity information is read during the preprocessing step of the simulation. The featured surface is the 600 x 600 μm^2 bottom XY plane. The mesh is deformed using the surface feature data. Figure 4(b) shows a detailed view of the cavities on multiple slices for a distribution shown in Figure 4(c). Five cavities with increasing diameters from 15 μm to 60 μm have been arranged in a canonical pattern that is representative of zones on a rough surface. The bottom surface is a constant temperature wall boundary held at a superheat of 5 K. The top surface is an outflow boundary, while the side boundaries are adiabatic walls. The cavity depth is fixed at 15 μm. The mesh consists of a total of 144,000 fourth-order elements, resulting in a problem with 9.2 million grid points. The temperature is set at saturation temperature (60°C) at time $t = 0$, along with zero velocity in the domain. Gravity is assumed to be in the vertical z direction perpendicular to the featured surface. The simulations took about 12 hours of wall clock time on 240 processors to run a 60-ms calculation. A constant time step of 5 μs was used in these simulations with a second-order backward Euler method for time integration. This time step was sufficient to perform stable simulations with maximum Courant numbers reaching a value of 0.5. Typically, the use of large Courant numbers greater than 1 results in numerical instabilities in our simulations. The importance of natural convection effects is first studied for this chosen distribution of cavities. Figure 5 shows the temperature transients for HFE7100 at four different times (2.5, 7, 15, and 17 ms). A cavity nucleates when the critical temperature given by Equation (5) is achieved. Three of the five cavities nucleate with natural convection effects as opposed to the central one being the only nucleated cavity for the case without natural convection. This difference is due to the greater transport of energy that results in cavities attaining their critical bubble temperature faster. Buoyancy-driven instability is clearly seen for the 15 ms and 17 ms snapshots, where lower density fluid rises and mixes with the colder, relatively denser medium.

The time at which each of the five cavities nucleates is plotted against cavity size in Figure 6. The cavities nucleate faster when natural convection effects are turned on (i.e., $\beta > 0$). This is due to the increased transport of energy via buoyant convection from the heated surface into the liquid phase. The 15 µm cavity tends to nucleate faster than the rest of the cavities in spite of its higher critical temperature requirement; this is due to the geometry of this relatively high aspect ratio cavity resulting in an increased temperature at the corresponding bubble height during the early temperature transients. For the case without natural convection, the cavities follow a trend where larger cavities nucleate slower compared to smaller ones. The larger cavities tend to nucleate approximately the same time for the case with natural convection. It should be noted that there are two competing effects that govern nucleation. The first parameter is the attainment of critical temperature given by Equation (5) and the second is the location at which the critical temperature needs to be attained. Although the critical temperature is lower for larger cavities that result in larger bubbles, longer time is required to transport the energy from the heated surface to the top of the bubble. This time lag is essentially reflected as increasing wait time for larger cavities in Figure 6 for the case without convection effects. For the case with natural convection effects, the buoyancy-driven plumes aid in efficient transport of energy from the heated surface; the onset of this instability leads to nucleation of the larger cavities at about the same time of ~17 ms.

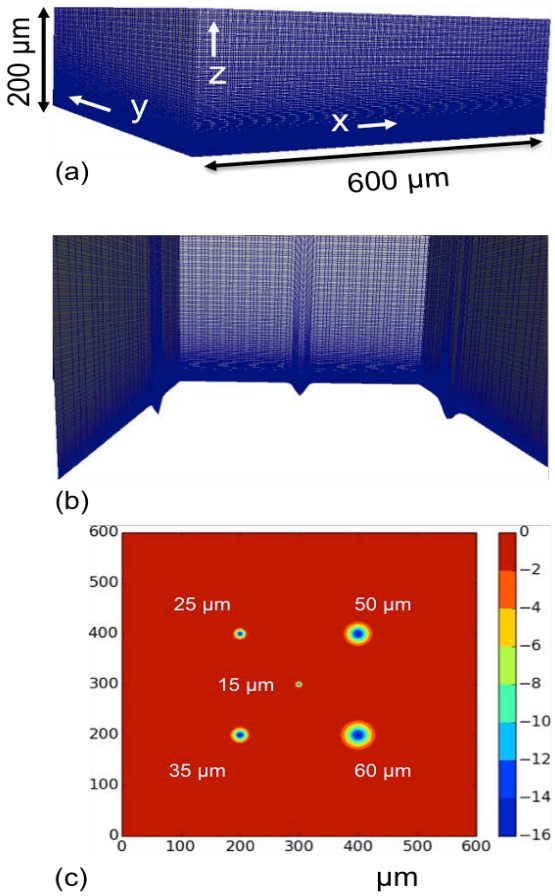

FIGURE 4: (a) SHOWS COMPUTATIONAL MESH FOR A BOX-LIKE DOMAIN CONSISTING OF 144,000 4th ORDER ELEMENTS. A CLOSE-UP VIEW OF CAVITIES ON MULTIPLE XZ AND YZ PLANES IS SHOWN IN (b), AND (c) DEPICTS A CONTOUR PLOT COLORED BY DEPTH OF FIVE DIFFERENT CAVITIES ON THE XY PLANE USED IN THIS STUDY.

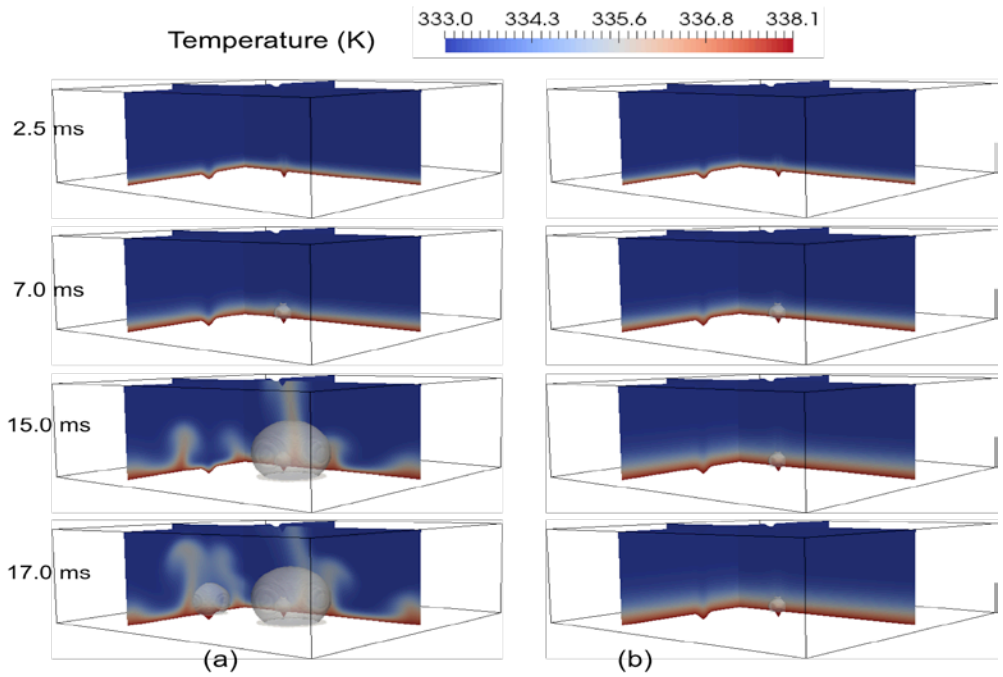

FIGURE 5: TRANSIENTS IMAGES OF TEMPERATURE DISTRIBUTION ON TWO ORTHOGONAL SLICES FOR CASES (a) WITH NATURAL CONVECTION, AND (b) WITHOUT NATURAL CONVECTION, RESPECTIVELY. THE GAS FRACTION CONTOURS ARE ALSO VISUALIZED TO DEPICT THE FORMATION OF VAPOR BUBBLES ON NUCLEATED CAVITIES.

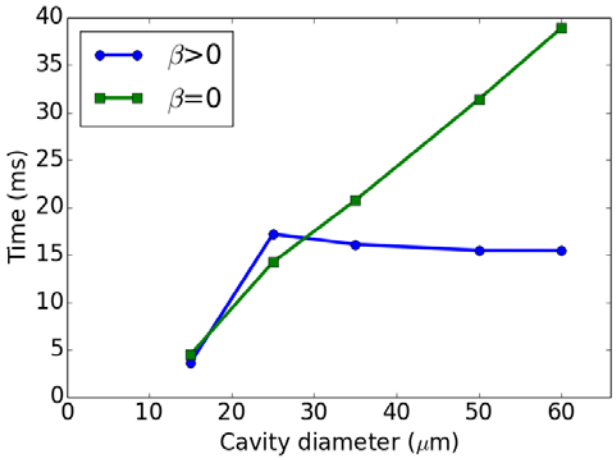

FIGURE 6: TIME OF CAVITY NUCLEATION PLOTTED AGAINST CAVITY SIZES FOR CASES WITH AND WITHOUT NATURAL CONVECTION. β IS THE VOLUME THERMAL EXPANSION COEFFICIENT.

Figure 7 shows the streamlines on two planes passing through the cavities for simulations performed with buoyant convection effects. Convection cells are observed to be formed with surface temperature variations caused by interactions with the surface geometry. High-velocity regions indicate formation and movement of buoyancy-driven plumes formed at the edge of the cavities. The Rayleigh number, Ra, for these simulations can be calculated using the definition in Equation 7:

$$Ra = \frac{g\beta}{\nu\alpha}(T_w - T_s)l^3 \qquad (7)$$

where g is the acceleration due to gravity, α is the thermal diffusivity, and T_w is the wall temperature. For a superheat of 5 K, transport properties from Table 1, and length scale, l = 0.2 mm (i.e., the domain length in the direction of gravity), the Rayleigh number is approximately 128. The critical Rayleigh number that determines the onset of natural convection in the idealized case is typically ~1,000, as derived from linearized theory [34], which is appreciably larger than the value calculated here. However, these simulations demonstrate a case with non-linear forcing due to the variation of temperature brought about by the surface geometry. It has been observed that convection is unavoidable—temperature forcing for any value of Rayleigh number [35] resulted in forced convection cells.

The formation of natural convection cells is consistent with recent experimental studies on heat transfer enhancement using bi-conductive materials [28]; surfaces with alternating low and high conductivity zones resulted in a non-uniform temperature

forcing, which in turn altered bubble dynamics and nucleation events.

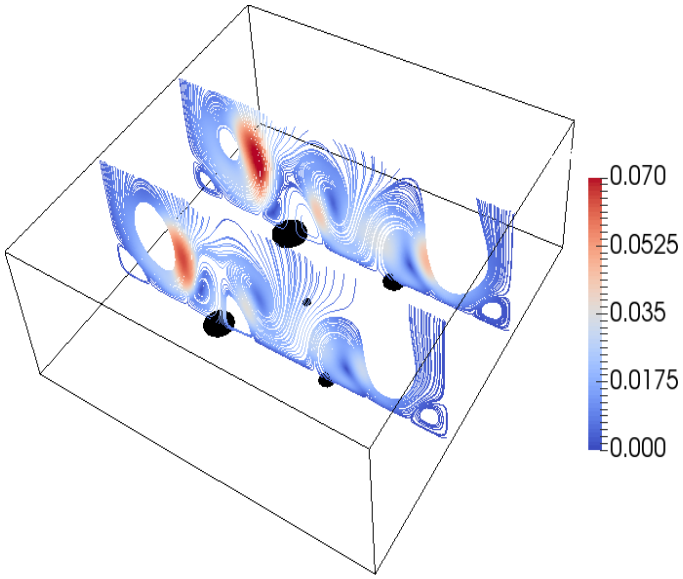

FIGURE 7: STREAMLINES COLORED BY MAGNITUDE OF VELOCITY IN METERS PER SECOND ON TWO PLANES AT TIME *t* = 17 ms. THE DARK SPOTS ON THE BOTTOM PLANE INDICATE THE CAVITIES.

3.2 Nucleation on Rough Surface

Simulation results pertaining to the generic rough surface described in Section 2.2 on cavity detection are presented here. These simulations are performed on a 2x2x0.6 mm^3 domain using 200,000 fourth-order elements with the same initial and boundary conditions for the featured surface simulations. A constant time step of 5 μs was used in these simulations. Figure 8 shows snapshots of the temperature distribution and isosurface (at 333 K) for a simulation of the rough surface kept at a superheat of 10 K. Figure 8(a) shows the temperature distribution on a plane close to the surface; perturbations on the order of 2 K are seen due to the presence of the micrometer features. These perturbations trigger buoyancy-driven plumes as shown in Figure 8(b). The plumes are observed to originate in the regions of higher temperature, Figure 8(a), where the fluid density is lower. The tips of the plumes have higher velocities opposite to the direction of gravity while the rest of the region has a negative *z*-direction component of velocity, resulting in recirculating convection cells.

Figure 9 shows an analysis pertaining to cavity nucleation over time and its dependence on wall superheat. The total number of cavities that have been nucleated at a given time is shown in Figure 9(a) for varying wall superheat. The onset of nucleation is logically delayed for lower values of superheat; for example, it takes ~15 ms for the 2 K superheat case, while it is almost instantaneous for the 5 K and 10 K cases.

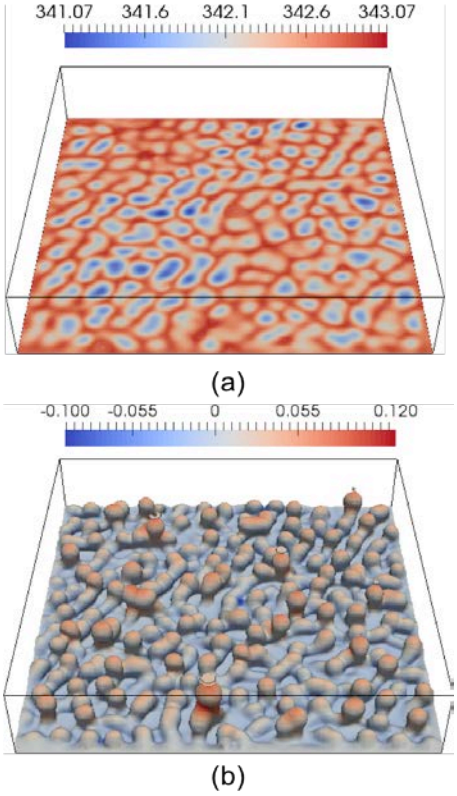

FIGURE 8: (a) SHOWS TEMPERATURE DISTRIBUTION IN K ON A PLANE CLOSE TO THE ROUGH SURFACE, AND (b) SHOWS ISOSURFACE OF TEMPERATURE AT 333 K COLORED BY THE *Z* COMPONENT OF VELOCITY IN METERS PER SECOND. THESE SNAPSHOTS ARE AT TIME *t* = 9 ms. THE SURFACE TEMPERATURE IS AT A SUPERHEAT OF 10 K.

This delay is associated with the time scale of attaining the critical bubble temperature via conduction and convection effects. The curves show a general trend, where there is a rapid increase in the number of active cavities early on leading to a steady value.

The rapid increase is associated with the nucleation of several small cavities whose critical temperatures are easily attained during transient heat transfer for higher superheats. These small cavities do not nucleate for lower superheats due to the unattainable critical temperature requirement. The steady value of the total number of active cavities also increases with higher wall superheat; for example, all of the 144 cavities have nucleated at the end of 30 ms for the 10 K superheat case.

Figure 9(b) shows the trend pertaining to the smallest cavity that is nucleated with varying superheats. The small wall superheat; for example, all of the 144 cavities have nucleated at the end of 30 ms for the 10 K superheat case.

Figure 9(b) shows the trend pertaining to the smallest cavity that is nucleated with varying superheats. The small

cavity sizes are important due to their large number (Figure 3(c)) and the higher critical temperature required for nucleation; note that Equation (5) shows an inverse proportionality to cavity radius. The size of the smallest cavity that is nucleated reduces with increasing superheat; higher wall superheat results in the attainment of critical temperature for smaller cavities, which is otherwise not possible at low superheats. It should be noted that this trend might seem contrary to the results presented in Section 3.1 on featured surfaces where the smallest cavity was the first to be activated. The simulations in Section 3.1 were performed using a constant wall superheat of 5 K, which was higher than the critical bubble temperature for the small cavity, while Figure 9 shows cases where the wall superheat is varied, resulting in situations where the critical temperature for small cavities are never attained. This trend is consistent with limiting cavity sizes predicted by Hsu's [29] nucleation model. It should be noted that the current work shows the trend of actual cavity sizes nucleated at different superheats while Hsu's model predicts the limiting cavity sizes that nucleate at infinite time. A similar trend was also observed in the studies by Chang and You [37] on boiling heat transfer from porous and microporous surfaces. Microporous coatings with smaller particle diameters, which resulted in smaller cavities, required higher superheat for incipience.

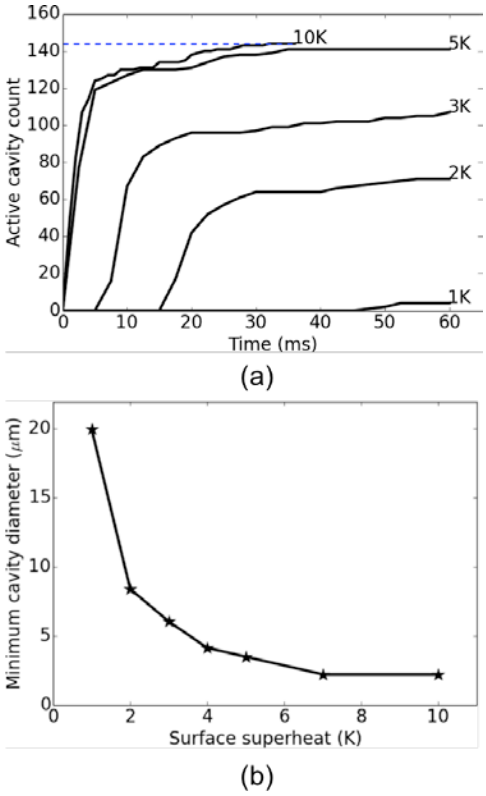

FIGURE 9: (a) SHOWS THE TOTAL NUMBER OF ACTIVE CAVITIES AS A FUNCTION OF TIME WITH VARYING SURFACE SUPERHEAT OF 1 K TO 10 K. THE BLUE DOTTED LINE INDICATES THE TOTAL NUMBER OF CAVITIES. (b) PLOTS THE MINIMUM SIZE CAVITY THAT IS ACTIVATED AT VARYING SURFACE SUPERHEAT CASES.

3.3 Grid Convergence Study

The featured surface simulations presented in Section 3.1 was repeated on multiple grid resolutions to show grid convergence of our simulations. The number of cells in the computational domain shown in Figure 4(a) was varied from 72,000 cells to 288,000 cells. It should be noted that the baseline simulations presented in Section 3.1 used a resolution of 144,000 cells. The cavity activation times converge to the same result for higher resolution cases as shown in Figure 10(a). Figures 10(b), (c), and (d) show the temperature field on a plane through two of the cavities on the featured surface for varying grid resolutions. The higher-resolution cases (144,000 cells and higher) show identical results, thus proving our simulations to be grid independent.

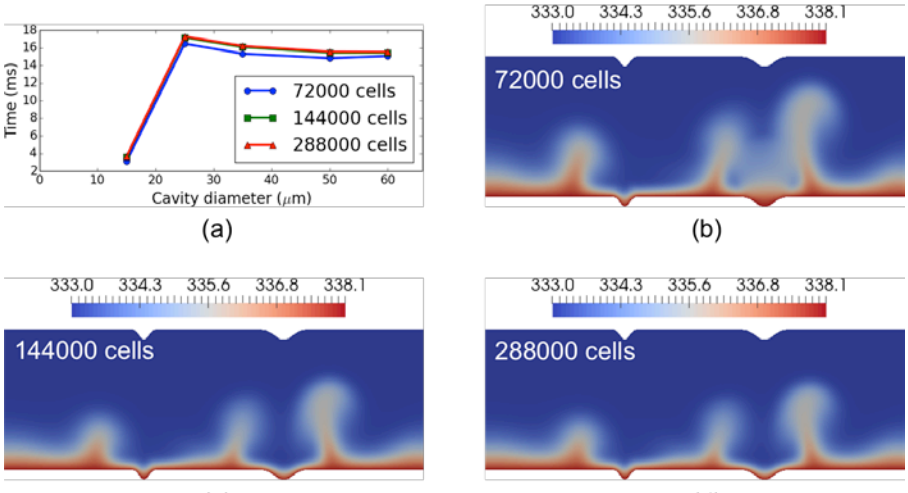

FIGURE 10: (a) SHOWS THE CAVITY ACTIVATION TIME VERSUS CAVITY SIZE FOR THE FEATURED SURFACE SIMULATIONS FOR VARYING GRID RESOLUTIONS. (b), (c), AND (d) SHOW TEMPERATURE SNAPSHOTS AT TIME t = 15 ms ON AN XZ PLANE WITH CAVITIES 25 AND 50 μm FOR 72,000, 144,000, AND 288,000 CELLS, RESPECTIVELY.

4. CONCLUSIONS AND FUTURE WORK

A high-fidelity model for studying the early stages of nucleate boiling has been developed in this work. A CFD model that includes the detailed surface morphology obtained via an image processing and cavity detection technique has been employed. The simulation results show the importance of natural convection and its effect on bubble nucleation. Simulations of a generic rough surface revealed that higher superheat is required to nucleate smaller-size cavities. The non-uniform temperature profile generated by the morphology of the rough surface leads to formation of buoyancy-driven plumes from high-temperature zones.

Future efforts will include the following:

1) One of the important model assumptions is regarding the presence of initial bubble nuclei in all cavities. This assumption needs further evaluation for highly wetting fluids and surfaces. This will require an *a priori* classification of cavities with and without a vapor nucleus. A statistical correlation can potentially be used to seed certain cavities according to the cavity size and fluid wettability.
2) This local micro- to millimeter-scale model can be potential coupled with an intermediate-scale VOF model. In this scenario, the local-scale model provides the initial conditions for the VOF model with locations and radii of nucleated bubbles. The VOF will then be used to simulate departure of these bubbles, which in turn modifies the fluid velocities and temperature in the vicinity of the featured surface. This information will be relayed back to the local-scale model to locate newly nucleated bubbles. This will provide additional insights on the later stages of nucleate boiling. Secondary effects such as the effect of bubble coalescence and shielding of cavities on nucleation can also be studied.
3) This model needs to be validated with experiments. Cavities fabricated using focused ion beam manufacturing will be used in experimental studies by the authors. High-speed videos of bubble nucleation will then be used to validate our model. The model will also be tested against constant heat flux cases (easily measured in experiments) instead of the constant temperature boundary used in this work. This will result in transient local variations of surface temperature and Rayleigh number, which may result in a different trend in cavity nucleation over time.

NOMENCLATURE

C	Average specific heat (J/K/kg)
$\boldsymbol{g}$	Acceleration due to gravity (m/s^2)
k	Average thermal conductivity (W/m/K)
L	Latent heat of vaporization (J/kg)
p	Pressure (Pa)
R	Bubble radius (m)
R_c	Cavity radius (m)
Ra	Rayleigh number
T	Fluid temperature (K)
T_b	Critical bubble temperature (K)
T_s	Saturation temperature (K)
T_w	Wall temperature (K)
$\boldsymbol{u}$	Fluid velocity (m/s)
α_l	Liquid volume fraction
α_g	Gas volume fraction
β	Thermal expansion coefficient (K^{-1})
μ	Average transport property
μ_l	Transport property (liquid)
μ_g	Transport property (gas)
ν	Kinematic viscosity (m^2/s)
ρ	Average mass density (kg/m^3)
ρ_g	Gas/vapor density (kg/m^3)
σ	Surface tension (N/m)
ϕ	Contact angle
σ	Surface tension (N/m)

ACKNOWLEDGMENTS

We acknowledge funding for this work from Toyota Engineering and Manufacturing of North America. This work also utilized high-performance-computing resources at the National Renewable Energy Laboratory (NREL), for which we are deeply grateful. The U.S. Government retains and the publisher, by accepting the article for publication, acknowledges that the U.S. Government retains a nonexclusive, paid-up, irrevocable, worldwide license to publish or reproduce the published form of this work, or allow others to do so, for U.S. Government purposes.

REFERENCES

[1] S. F. Jones, G. M. Galvin, K. P. Evans, "Bubble nucleation from gas cavities a review ," *Advances in Colloid and Interface Science* , vol. 80, pp. 27-50, 1999.

[2] M Blander and J. L. Katz, "Bubble Nucleation in Liquids," *AIChE Journal*, vol. 21, no. 5, pp. 833-848, 1975.

[3] M. Jacob and W Fritz, "Versuche uber den verdampfungsvorgang," *Forschung auf dem Gebiete des Ingenieurwesens* , vol. 2, pp. 435-437, 1931.

[4] P. Griffith and J. D. Wallis, "The Role of surface conditions in nucleate boiling," *Chemical Engineering Progress symposium series*, vol. 56, no. 49, pp. 49-63, 1960.

[5] J. E. Benjamin, "Bubble growth in nucleate boiling of a binary mixture," Chemistry and Chemical Engineering, University of Illinois at Urbana-Champaign, PhD Thesis 1961.

[6] R. L. Webb, "Heat transfer surface having a high boiling heat transfer coefficient," US3696861 A, October 10, 1972.

[7] T. J. Hendricks, S. Krishnan, C. Choi, C-H. Chang, and B. Paul, “Enhancement of pool-boiling heat transfer using nanostructured surfaces on aluminum and copper ,” *International Journal of Heat and Mass Transfer* , vol. 53, pp. 3357-3365, 2010.

[8] J. McHale, S. V. Garimalla, T. S. Fisher, and G. A. Powell, “Pool boiling performance comparison of smooth and sintered copper surfaces with and without carbon nanotubes ,” *Nanoscale and Microscale Thermophysical Engineering* , vol. 15, no. 3, pp. 133-150, 2011.

[9] A. K Das, P.K. Das, and P. Saha, “Nucleate boiling of water from plain and structured surfaces ,” *Experimental Thermal and Fluid Science* , vol. 31, pp. 967-977, 2007.

[10] G. Moreno, J. Jeffers, and S. Narumanchi, “Effects of pressure and a microporous coating on HFC-245fa pool boiling heat transfer,” *ASME Journal of Heat Transfer*, vol. 136, no. 101502, 2014.

[11] G. Moreno, S. Narumanchi, and C. King, “Pool boiling heat transfer characteristics of HFO-1234yf on plain and microporous-enhanced surfaces," *ASME Journal of Heat Transfer*, vol. 135, no. 111014, 2013.

[12] S. Thiagarajan, R. Yang, C. King, and S. Narumanchi, "Bubble dynamics and nucleate pool boiling heat transfer on microporous copper surfaces," *International Journal of Heat and Mass Transfer*, vol. 89, pp. 1297-1315.

[13] M. S. El-Genk and A. F. Ali, "Enhanced nucleate boiling on copper micro-porous surfaces ," *International Journal of Multiphase Flow* , vol. 36, pp. 780-792, 2010.

[14] A.K. Das, P.K. Das, and P Saha, "Some investigations on the enhancement of boiling heat transfer from planer surface embedded with continuous open tunnels," *Experimental Thermal and Fluid Science*, vol. 34, pp. 1422-1431, 2010.

[15] D. S. Jung, J. E. S. Venart, and A. C. M. Sousa, "Effects of enhanced surfaces and surface orientation on nucleate and film boiling heat transfer in R-11," *International Journal of Heat and Mass Transfer*, vol. 30, no. 12, pp. 2627-2639, 1987.

[16] S. Ujereh, T. Fisher, and I. Mudawar, "Effects of carbon nanotube arrays on nucleate pool boiling ," *International Journal of Heat and Mass Transfer*, vol. 50, pp. 4023-4038, 2007.

[17] C. Kunkelmann and P. Stephan, "CFD Simulation of Boiling Flows Using the Volume- of-Fluid Method within OpenFOAM ," *Numerical Heat Transfer, Part A: Applications* , vol. 56, no. 8, pp. 631-646, 2009.

[18] C. Fang, M. David, A. Rogacs, and K. Goodson, "Volume of fluid simulation of boiling two-phase flow in a vapor-venting microchannel ," *Frontiers in Heat and Mass Transfer* , vol. 1, p. 013002, 2010.

[19] J. Wu, V. K. Dhir, and J. Qian, "Numerical Simulation of Subcooled Nucleate Boiling by Coupling Level-Set Method with Moving- Mesh Method ," *Numerical Heat Transfer, Part B: Fundamentals* , vol. 51, pp. 535-563, 2007.

[20] K. Ling, Z-Y. Li, and W-Q. Tao, "A direct numerical simulation for nucleate boiling by the method ," *Numerical Heat Transfer, Part A*, vol. 65, pp. 949-971, 2014.

[21] M. Yazdani, T. Radcli, M. Soteriou, and A. A. Alahyari, "A high-delity approach towards simulation of pool boiling ," *Physics of Fluids*, vol. 28, no. 012111, 2016.

[22] Y. Sato and B. Niceno, "Nucleate pool boiling simulations using the interface tracking method: Boiling regime from discrete bubble to vapor mushroom region ," *International Journal of Heat and Mass Transfer* , vol. 105, pp. 505-524, 2017.

[23] J. Liu and T. Hughes, "Isogeometric Phase-Field Simulation of Boiling," in *Advances in Computational Fluid-Structure Interaction and Flow Simulation*., 2016, pp. 217-228.

[24] S. Narumanchi, A. Troshko, D. Bharathan, and V. Hassani, "Numerical simulations of nucleate boiling in impinging jets: Applications in power electronics cooling," *International Journal of Heat and Mass Transfer*, vol. 51, pp. 1-12, 2008.

[25] W. E. Ranz and W. R. Marshall, "Evaporation from drops," *Chemical Engineering Progress*, vol. 48, no. 3, pp. 141-146, 1952.

[26] H. Li, S. A. Vasquez, H. Punekar, and R. Muralikrishnan, "Prediction of boiling and critical heat flux using an Eulerian Multiphase Boiling Model," in *Proceedings of the ASME 2011 International Mechanical Engineering Congress & Exposition*, Denver, 2011.

[27] S. Gong and P. Cheng, "Lattice Boltzmann simulation of periodic bubble nucleation, growth and departure from a heated surface in pool boiling ," *International Journal of Heat and Mass Transfer* , vol. 64, pp. 122-132, 2013.

[28] S. Maruyama and T. Kimura, "A Molecular Dynamics Simulation of a Bubble Nucleation on Solid Surface ," in *5th ASME/JSME Joint Thermal Engineering Conference* , vol. AJTE99-6511 , San Diego, 1999.

[29] Y. Y. Hsu, "On the size range of active nucleation cavities on a heating surface.," *ASME Journal of Heat Transfer*, pp. 207-216, 1962.

[30] P. F. Fischer, J. W. Lottes, and S. G. Kerkemeier. (2008) nek5000 Web page. [Online]. http://nek5000.mcs.anl.gov

[31] I. Mudawar, "Spray cooling of power electronics and technical support for advanced power electronics ," Mudawar thermal systems, West Lafayette, IN, Technical Report 2006.

[32] R. W. Johnson, *Handbook of fluid dynamics*.: CRC press, 2016.

[33] C. Kunkelmann, "Numerical Modeling and Investigation of Boiling Phenomena ," PhD Thesis 2011.

[34] S. Chandrasekhar, *Hydrodynamic and Hydromagnetic Stability*.: Dover, 1961.

[35] G. Freund, W. Pesch, and W. Zimmermann, "Rayleigh–Be´nard convection in the presence of spatial temperature modulations ," *Journal of Fluid Mechanics*, vol. 673, pp. 318-348, 2011.

[36] M. M. Rahman, J. Pollack, and M. McCarthy, "Increasing boiling heat transfer using low conductivity materials," *Scientific reports*, vol. 5, p. 13145, 2015.

[37] J. Y. Chang and S. M. You, "Boiling heat transfer phenomena from micro- porous and porous surfaces in saturated FC-72 ," *Int. J Heat and Mass Transfer*, vol. 40, no. 18, pp. 4437-4447, 1997.